More indications for lepton nonuniversality in $b \to s\ell+\ell-$

T. Hurth, F. Mahmoudi, D. Martínez Santos, S. Neshatpour

CERN-TH-2021-064, MITP/21-020

More Indications for Lepton Nonuniversality in $b \to s\ell^+\ell^-$

T. Hurth[a], **F. Mahmoudi**[b,c], **D. Martínez Santos**[d], **S. Neshatpour**[b]

[a] *PRISMA+ Cluster of Excellence and Institute for Physics (THEP), Johannes Gutenberg University, D-55099 Mainz, Germany*

[b] *Université de Lyon, Université Claude Bernard Lyon 1, CNRS/IN2P3, Institut de Physique des 2 Infinis de Lyon, UMR 5822, F-69622, Villeurbanne, France*

[c] *Theoretical Physics Department, CERN, CH-1211 Geneva 23, Switzerland*

[d] *Instituto Galego de Física de Altas Enerxías, Universidade de Santiago de Compostela, Spain*

ABSTRACT

Recently the LHCb collaboration has confirmed the evidence for lepton flavour nonuniversality at the 3.1σ level via an updated measurement of R_K. In this work we analyse this evidence within a model-independent approach. We make projections for future measurements which indicate that LHCb will be in the position to discover lepton nonuniversality with the Run 3 data in a single observable. We analyse other ratios based on our analysis of the present measurements of the ratios $R_{K^{(*)}}$ and analyse if they are able to differentiate between various new physics options within the effective field theory at present or in the near future. We also compare the present deviations in the ratios with NP indications in the angular observables of exclusive $b \to s\ell\ell$ transitions. Finally, we update our global analysis considering all $b \to s\ell\ell$ observables altogether, including a 20-parameter fit in connection of a Wilks' test.

1 Introduction

Ever since the measurement of the full angular observables of the exclusive $B \to K^* \mu^+ \mu^-$ decay with 1 fb^{-1} data by LHCb [1] which suggested that there may be signs of New Physics (NP) in C_9^μ [2–6], rare $b \to s$ observables have been showing the strongest hints for NP. Updated measurements of the $B \to K^* \mu^+ \mu^-$ angular observables by the LHCb experiment with 3 and 4.7 fb^{-1} data [7, 8] as well as measurements in other exclusive modes such as $B_s \to \phi \mu^+ \mu^-$ [9] have indicated potential signs of NP (with deviations of more than 2σ for some observables/bins). Although the SM predictions of some of the angular observables of the aforementioned modes have rather small uncertainties, in general the observables of the exclusive decays suffer from hadronic uncertainties, which often do not allow us to confidently separate possible NP effects from hadronic effects.

Another group of rare decays which have shown signs of NP are lepton flavour universality violating (LFUV) observables $R_{K^{(*)}} \equiv \text{BR}(B^{+(0*)} \to K^{+(0*)} \mu^+ \mu^-)/\text{BR}(B^{+(0*)} \to K^{+(0*)} e^+ e^-)$ [10] where the ratios of the branching fractions of muons compared to electrons are considered. The LFUV observables are theoretically very clean with SM uncertainties less than one percent[1]. The first tension in LFUV observables was measured for R_K in the $[1.1, 6.0]$ GeV^2 bin with the LHCb Run-1 data with 2.6σ significance [12]. This tension was confirmed with a significance of 2.5σ when combining the Run 2 and the re-optimised Run 1 result [13] which had smaller uncertainty although the central value was measured to be closer to the SM prediction. LHCb found similar tensions at the level of 2.3 and 2.5σ for R_{K^*} in the two low-q^2 bins $[0.045, 1.1]$ and $[1.1, 6.0]$ GeV^2, respectively [14]. These tensions within the theoretically clean ratios were shown to be rather consistent with the previously found tensions in the angular observables [15–18].

Among the non-LFUV observables, the $\text{BR}(B_s \to \mu^+ \mu^-)$ is one of the cleanest observables giving a very good handle on the muon sector without involving the electron sector. Moreover, assuming no NP contributions due to scalar and pseudo-scalar operators (which is indicated by $b \to s \ell^+ \ell^-$ global fits), the short-distance contribution to this decay is only via $C_{10}^{\mu(\prime)}$.

Recently LHCb has updated two of the clean observables, namely R_K and $BR(B_s \to \mu^+ \mu^-)$ using the complete dataset collected so far [19–21]. The LHCb experiment measures 3.1σ tension with the SM prediction for R_K

$$R_K^{\text{LHCb}}([1.1, 6.0] \text{ GeV}^2) = 0.846^{+0.042+0.013}_{-0.039-0.012}\,, \tag{1}$$

which compared to the previous result with 5 fb^{-1} data [13] has exactly the same central value but now due to smaller experimental uncertainties has an increased tension with the SM. The new LHCb measurement of $\text{BR}(B_s \to \mu^+ \mu^-)$ gives [19, 20]

$$\text{BR}(B_s \to \mu^+ \mu^-)^{\text{LHCb}} = (3.09^{+0.46+0.15}_{-0.43-0.11}) \times 10^{-9}\,. \tag{2}$$

In our fits, for the experimental value of $\text{BR}(B_s \to \mu^+ \mu^-)$ we combine the recent LHCb update [19, 20] with the ATLAS [22] and CMS [23] results as shown in Fig. 1, where a 2D likelihood is obtained by making a joint likelihood from the published contours of the 3 experiments while taking the ratio of hadronisation fractions and the $\text{BR}(B^+ \to J/\psi K^+)$ as correlated systematics. For the combined experimental measurement of the $B_s \to \mu^+ \mu^-$ decay we have

$$\text{BR}(B_s \to \mu^+ \mu^-)^{\text{exp(comb.)}} = (2.85^{+0.34}_{-0.31}) \times 10^{-9}\,. \tag{3}$$

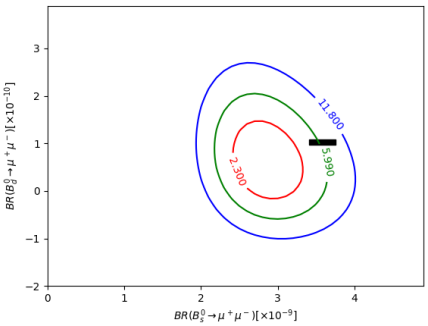

Figure 1: 2D likelihood plot of $\text{BR}(B_{s,d} \to \mu^+ \mu^-)$.

[1] Only for the very low $q^2 \in [0.045, 1.1]$ GeV^2 bin of R_{K^*} one finds an uncertainty of $\sim 3\%$ [11].

In the next section we discuss the impact of the recent LHCb measurements on the fit to clean observables and investigate in detail the role of $\mathrm{BR}(B_s \to \mu^+\mu^-)$ in the two-dimensional fit to LFUV observables. We also analyse the consistency of the clean observables and the rest of the $b \to s\ell\ell$ data regarding new physics. In section 3 we update our global $b \to s\ell\ell$ analysis in a multidimensional New Physics fit and consider the Wilks' test. In section 4, we present the future prospects of the clean observables, and make predictions for further ratios. The conclusions are given in section 5.

2 New physics analysis

In this section we consider the new physics analysis of $R_{K^{(*)}}$ and $\mathrm{BR}(B_{s,d} \to \mu^+\mu^-)$ and compare with other $b \to s$ data. The nonfactorisable power corrections in exclusive $b \to s\ell\ell$ decays are not completely under control and have to be guesstimated. The correct parametrisation of these unknown power-corrections were presented in Refs. [24,25]. Instead of guesstimating their size, these hadronic corrections can be directly fitted to the data as an alternative explanation of the tensions [26–29]. Although promising approaches like the one in Ref. [30] may solve this problem in the near future (see Ref. [31] for recent progress), it is still reasonable to make separate analyses of the theoretically very clean ratios and the other $b \to s$ observables to crosscheck the consistency of the two data sets.

2.1 NP fit to clean observables

In Table 1 the results of the one operator fits to new physics using only the data on the seven measurements, R_K (the $[1.1, 6]$ bin from LHCb [21]), R_{K^*} (the $[0.045, 1.1]$ and $[1.1, 6]$ bins from LHCb [14] and the $[0.1, 8]$ and $[15, 19]$ bins from Belle [32]) and $B_{s,d} \to \mu\mu$ (our combination) are shown where for our analysis we have used the `SuperIso` public program [33]. The second columns in Table 1 correspond to the best fit (b.f.) value ± 68% confidence intervals. With the updated (2021) data, the p-value of the SM is 0.02%, while the p-value of the most favoured one-dimensional NP fit (C^μ_{LL}) is 31.2%. Compared to our 2019 fits in Ref. [34] we see increased significances for the NP fits to the theoretically clean ratios R_K and R_{K^*}. In general, the SM pull of the one operator fits are changed by more than 1σ. This is clearly due to the increased tension of the recent R_K measurement with the SM. Our findings are in agreement with the recent model-independent analyses in Refs. [35–38].

Only $R_K, R_{K^*}, B_{s,d} \to \mu^+\mu^-$ **2019 data** ($\chi^2_{\mathrm{SM}} = 19.0$)			
	b.f. value	χ^2_{min}	$\mathrm{Pull}_{\mathrm{SM}}$
δC_9	-2.04 ± 5.93	18.9	0.3σ
δC_9^e	0.79 ± 0.29	9.9	3.0σ
δC_9^μ	-0.74 ± 0.28	10.6	2.9σ
δC_{10}	0.43 ± 0.32	17.0	1.4σ
δC_{10}^e	-0.78 ± 0.27	8.2	3.3σ
δC_{10}^μ	0.65 ± 0.20	6.9	3.5σ
δC_{LL}^e	0.41 ± 0.15	9.0	3.2σ
$\delta C_{\mathrm{LL}}^\mu$	-0.37 ± 0.11	7.2	3.4σ

Only $R_{K^{(*)}}, B_{s,d} \to \mu^+\mu^-$ **2021 data** ($\chi^2_{\mathrm{SM}} = 28.19$)			
	b.f. value	χ^2_{min}	$\mathrm{Pull}_{\mathrm{SM}}$
δC_9	-1.00 ± 6.00	28.1	0.2σ
δC_9^e	0.80 ± 0.21	11.2	4.1σ
δC_9^μ	-0.77 ± 0.21	11.9	4.0σ
δC_{10}	0.43 ± 0.24	24.6	1.9σ
δC_{10}^e	-0.78 ± 0.20	9.5	4.3σ
δC_{10}^μ	0.64 ± 0.15	7.3	4.6σ
δC_{LL}^e	0.41 ± 0.11	10.3	4.2σ
$\delta C_{\mathrm{LL}}^\mu$	-0.38 ± 0.09	7.1	4.6σ

Table 1: Comparison of one operator NP fits with 2019 and 2021 data on R_K, R_{K^*} and $\mathrm{BR}(B_{s,d} \to \mu^+\mu^-)$.

2.2 NP fit to all $b \to s$ observables except $R_{K^{(*)}}$ and $B_{s,d} \to \mu\mu$

For the rest of the $b \to s\ell^+\ell^-$ observables (except R_K, R_{K^*} and $B_{s,d} \to \mu\mu$), we also find larger SM pulls of the one operator fits compared to the analysis in Ref [34]. As shown in Table 2, there is a $1-2\sigma$ increase of the SM pull which is due to a new measurement of the angular observables of the $B^0 \to K^{*0}\mu^+\mu^-$ decay (see Ref [39] for more details) and due to the inclusion of further observables such as the angular observables of the charged $B^+ \to K^{*+}\mu^+\mu^-$ decay (see Ref. [40]) and the branching ratio and angular observables of the $\Lambda_b \to \Lambda\mu^+\mu^-$ baryonic decays[2]. With this set of observables, the 3.6% p-value of the

[2]The complete list of considered observables amount to 166 observables which include the isospin symmetry breaking and the branching ratio of $B \to K^*\gamma$, and the branching ratios of $B_s \to K^*e^+e^-$, $B_s \to e^+e^-$ and $B^0 \to K^0\mu^+\mu^-$, where for the latter decay the 2 low- and high-q^2 bins have been taken into account. For the inclusive modes, the branching ratios of $B \to X_s\gamma$, $B \to X_se^+e^-$ and $B \to X_s\mu^+\mu^-$ where for the two latter we have considered the low- and high-q^2 bins. For the $B^+ \to K^+\mu^+\mu^-$ decay we have included the branching ratio and F_H in the two low- and high-q^2 bins. For the $B \to K^*\mu^+\mu^-$ decay the branching ratio and the angular observables $(F_L, A_{FB}, S_{3,4,5,7,8,9})$ in the 5 low- and 2 high-q^2 bins have been taken into account. The angular observables $(F_L, S_{3,4,7})$ and branching ratio of $B_s \to \phi\mu^+\mu^-$ have been considered in 3 low- and 2 high-q^2 bins. For the $B^+ \to K^{*+}\mu^+\mu^-$ decay we consider the branching ratio for the two low- and high-q^2 bins and the angular observables $(F_L, A_{FB}, S_{3,4,5,7,8,9})$ in the 5 low- and 2 high-q^2 bins. We have also included the branching ratio and angular observables $(A^\ell_{FB}, A^h_{FB}, A^{lh}_{FB}, F_L)$ for the baryon decay $\Lambda_b \to \Lambda\mu^+\mu^-$ in the high-q^2 bin.

All observables except $R_{K^{(*)}}, B_{s,d} \to \mu^+\mu^-$ **2019 data** ($\chi^2_{\rm SM} = 99.7$)			
	b.f. value	$\chi^2_{\rm min}$	Pull$_{\rm SM}$
δC_9	-1.03 ± 0.20	81.0	4.3σ
δC_9^e	0.72 ± 0.58	98.5	1.1σ
δC_9^μ	-1.05 ± 0.19	78.8	4.6σ
δC_{10}	0.27 ± 0.28	98.7	1.0σ
δC_{10}^e	-0.56 ± 0.50	98.7	1.0σ
δC_{10}^μ	0.38 ± 0.28	97.7	1.4σ
$\delta C_{\rm LL}^e$	0.33 ± 0.29	98.6	1.1σ
$\delta C_{\rm LL}^\mu$	-0.50 ± 0.16	88.8	3.3σ

All observables except $R_{K^{(*)}}, B_{s,d} \to \mu^+\mu^-$ **2021 data** ($\chi^2_{\rm SM} = 200.1$)			
	b.f. value	$\chi^2_{\rm min}$	Pull$_{\rm SM}$
δC_9	-1.01 ± 0.13	158.2	6.5σ
δC_9^e	0.70 ± 0.60	198.8	1.1σ
δC_9^μ	-1.03 ± 0.13	156.0	6.6σ
δC_{10}	0.34 ± 0.23	197.7	1.5σ
δC_{10}^e	-0.50 ± 0.50	199.0	1.0σ
δC_{10}^μ	0.41 ± 0.23	196.5	1.9σ
$\delta C_{\rm LL}^e$	0.33 ± 0.29	198.9	1.1σ
$\delta C_{\rm LL}^\mu$	-0.75 ± 0.13	167.9	5.7σ

Table 2: Comparison of one operator NP fits with 2019 and 2021 data on $b \to s\ell^+\ell^-$ transitions except R_K, R_{K^*}, BR$(B_{s,d} \to \mu^+\mu^-)$ assuming 10% error for the power corrections. The observable set used in 2019 fit on the left panel is not exactly the same as the 2021 one (e.g. $B^+ \to K^{*+}\mu^+\mu^-$ and $\Lambda_b \to \Lambda\mu^+\mu^-$ observables).

SM increases to 68% when having NP in C_9^μ as the most favoured 1-dimensional scenario. We emphasize again that the large SM-pulls beyond 5σ are based on guesstimates of the 10% nonfactorisable power corrections within the angular observables.

2.3 Coherence of clean observables with the rest of $b \to s$ observables

Comparing the right panels of Tables 1 and 2, while there are scenarios such as C_{LL}^μ for which the best fit point differ by more than 2σ, overall the one-dimensional fits are coherent in the preferred NP scenario whether the clean observables are considered for the fit, or the rest of the $b \to s\ell\ell$ data, indicating either a negative δC_9^μ or a positive δC_{10}^μ for both sets of observables in agreement within 1σ.

We also present two operator fits and analyse the role of the modes $B_{s,d} \to \mu^+\mu^-$: The coherence is not trivial in the two operator fits. In the fit to the clean observables it is crucial to also consider BR$(B_{s,d} \to \mu^+\mu^-)$ in order to get the correct sign for $\{C_9, C_{10}\}$ as shown in Fig. 2. Fit to R_K and R_{K^*} alone do not favour a sign for C_9^μ (the colored region of the right plot) and it is only after including BR$(B_{s,d} \to \mu^+\mu^-)$ (the black contour of the right plot) that similar best fit signs are obtained for the clean and the rest of the observables.

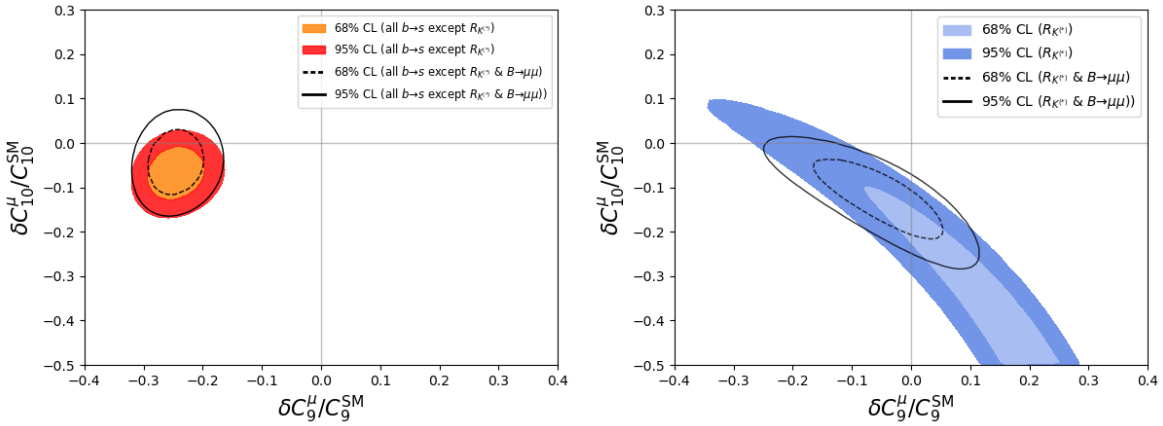

Figure 2: Two operator fits to $\{C_9^\mu, C_{10}^\mu\}$. On the left we have considered all observables except R_K and R_{K^*} with the assumption of 10% power corrections giving Pull$_{\rm SM} = 6.4\sigma$. On the right we have only used the data on R_K, R_{K^*} finding Pull$_{\rm SM} = 4.1\sigma$. The black dashed and solid contours correspond to excluding (including) the data on $B_{s,d} \to \mu^+\mu^-$ from (to) the fits of the left (right) plot where Pull$_{\rm SM}$ remains the same (becomes 4.2σ).

This feature is due to the degeneracy that the ratios $R_{K^{(*)}}$ have in C_9^μ and C_{10}^μ as can be seen by the circular contours of Fig. 3 where a positive δC_9^μ explains the data when simultaneously having a rather large value of δC_{10}^μ (not consistent with other $b \to s\ell\ell$ observables). The best fit value of the fit to only $R_{K^{(*)}}$ is $\{C_9^\mu, C_{10}^\mu\} = \{1.3 \pm 0.1, 4.0 \pm 4.0\}$ as indicated with the yellow diamond in Fig. 3 while when the BR$(B_{s,d} \to \mu^+\mu^-)$ is also included the best fit value is $\{C_9^\mu, C_{10}^\mu\} = \{-0.2 \pm 0.3, 0.5 \pm 0.2\}$ as indicated with a green cross.

It should be noted that the LHCb measured central value of R_{K^*} in the very low q^2 bin cannot be

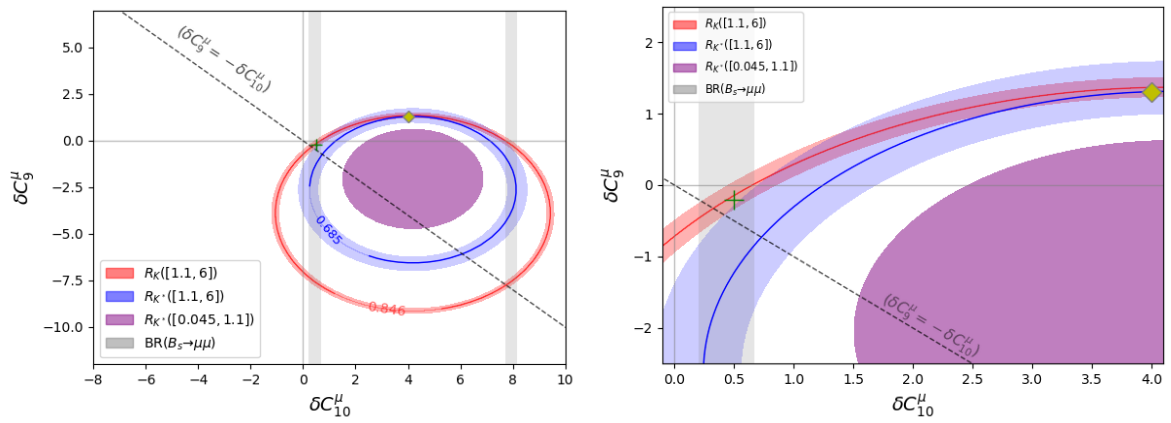

Figure 3: Clean observables within 1σ of experimental central value. The red (blue) solid line indicate the central value of the experimental measurements of $R_K^{[1.1,6]}$ ($R_{K^*}^{[1.1,6]}$). The colored regions give the 1σ range (theoretical and experimental uncertainties added in quadrature) with the experimental central value. The yellow diamond corresponds to the best fit point ($\{C_9^\mu, C_{10}^\mu\} = \{1.3 \pm 0.1, 4.0 \pm 4.0\}$) of the fit to only $R_{K^{(*)}}$ while the green cross indicates the best fit value ($\{C_9^\mu, C_{10}^\mu\} = \{-0.2 \pm 0.3, 0.5 \pm 0.2\}$) when fitting to $R_{K^{(*)}}$ and $\mathrm{BR}(B_{s,d} \to \mu^+\mu^-)$.

reached with any combination of NP in $\delta C_{9,10}^\mu$ since this bin is dominated by the photon contribution via the radiative Wilson coefficient C_7.

The comparison of the fits to the two separate sets of observables confirm our observations in previous analyses. Within the one operator fits the C_{10}-like Wilson coefficients play a significant role in the set of clean observables, but not in the complementary set. And the two operator fits in Figure 2 indicate that there is consistency between the two sets of observables at the 2σ level only.

3 Global fit

In the next step we show the global one and two operator fits in Table 3 and in Fig. 4 respectively using the $b \to s$ data altogether (observables of section 2.1 together with the ones from section 2.2 resulting in 173 observables in total). In the one operator fit, the hierarchy of the preferred NP scenarios have remained the same as is in 2019, with the most prominent scenario indicating beyond the SM contributions to the muon Wilson coefficient δC_9^μ followed by δC_{LL}^μ and the universal (not lepton flavour-dependent) Wilson coefficient δC_9. Considering the full set of $b \to s\ell\ell$ observables, the SM p-value is 0.4% while for the 1-dimensional fit to C_9^μ it increases to 55.9%. The significance of these scenarios have increased by more than 2σ compared to 2019 using the same 10% assumption for the power corrections. This increase is mainly due to the updated measurement of the $B^0 \to K^{*0}\mu^+\mu^-$ angular observables as well as the measurement of $B^+ \to K^{*+}\mu^+\mu^-$ and finally the recent LHCb measurements of R_K and $B_s \to \mu^+\mu^-$ where interestingly at each step the data has indicated the same preferred NP scenario (see also Refs. [39, 40]).

All observables **2019 data** ($\chi^2_{\rm SM} = 117.03$)			
	b.f. value	$\chi^2_{\rm min}$	$\mathrm{Pull}_{\rm SM}$
δC_9	-1.01 ± 0.20	99.2	4.2σ
δC_9^e	0.78 ± 0.26	106.6	3.2σ
δC_9^μ	-0.93 ± 0.17	89.4	5.3σ
δC_{10}	0.25 ± 0.23	115.7	1.1σ
δC_{10}^e	-0.73 ± 0.23	105.2	3.4σ
δC_{10}^μ	0.53 ± 0.17	105.8	3.3σ
$\delta C_{\rm LL}^e$	0.40 ± 0.13	105.8	3.3σ
$\delta C_{\rm LL}^\mu$	-0.41 ± 0.10	96.6	4.5σ

All observables **2021 data** ($\chi^2_{\rm SM} = 225.8$)			
	b.f. value	$\chi^2_{\rm min}$	$\mathrm{Pull}_{\rm SM}$
δC_9	-0.99 ± 0.13	186.2	6.3σ
δC_9^e	0.79 ± 0.20	207.7	4.3σ
δC_9^μ	-0.95 ± 0.12	168.6	7.6σ
δC_{10}	0.32 ± 0.18	222.3	1.9σ
δC_{10}^e	-0.74 ± 0.18	206.3	4.4σ
δC_{10}^μ	0.55 ± 0.13	205.2	4.5σ
$\delta C_{\rm LL}^e$	0.40 ± 0.10	206.9	4.3σ
$\delta C_{\rm LL}^\mu$	-0.49 ± 0.08	180.5	6.7σ

Table 3: Comparison of one operator NP fits with 2019 and 2021 data on all the relevant data on $b \to s$ transitions, assuming 10% error for the power corrections.

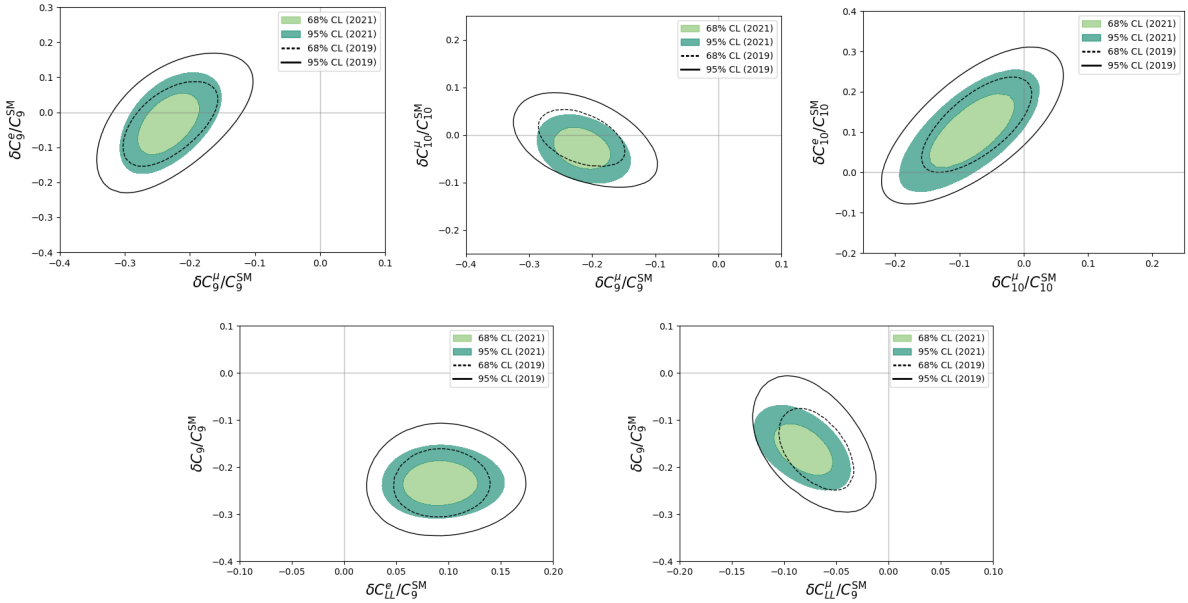

Figure 4: Two operator fits to NP, considering all observables (with the assumption of 10% power corrections). The colored bands (black contours) correspond to the 68 and 95% confidence level regions considering the 2021 (2019) data. $\text{Pull}_{\rm SM}$ in the $\{\delta C_9^e, \delta C_9^\mu\}, \{\delta C_{10}^\mu, \delta C_9^\mu\}, \{\delta C_{10}^e, \delta C_{10}^\mu\}$ fits are $7.3, 7.3, 4.5\sigma$, respectively. $\text{Pull}_{\rm SM}$ for the $\{\delta C_{LL}^e, \delta C_9\}$ and $\{\delta C_{LL}^\mu, \delta C_9\}$ fits of the lower row are 7.4 and 7.5σ, respectively.

For the two operator fit the most prominent scenario still involves a universal NP contribution to δC_9 together with δC_{LL}^μ very slightly preferred over δC_{LL}^e followed by NP in the $\{\delta C_9^e, \delta C_9^\mu\}$ and $\{\delta C_{10}^\mu, \delta C_9^\mu\}$ as given in the caption of Fig. 4. All the four mentioned scenarios have very similar $\text{Pull}_{\rm SM}$ and all involve a NP contribution to $\delta C_9^{(\mu)}$. Our results are in part consistent with, but also in part different from the results in the recent model-independent analyses in Refs. [35–37,41] (see also [42]). There are two obvious reasons which are responsible for larger discrepancies in the SM-pulls, namely different guesstimates of the nonfactorisable power corrections and different choices of the set of observables used in the fit. For the effect of enlargement of the hadronic uncertainties on the NP significances, see e.g. Refs. [35, 43].

In general NP contributions do not necessarily contribute to only one or two Wilson coefficients and could simultaneously involve several operator structures. In these cases the one and two operator fits lead to unnaturally large SM-pulls. Indeed, beyond simplified models, general NP scenarios contain a variety of new particles and new couplings. Therefore, taking a more agnostic approach to the behaviour of NP contributions, as first proposed in Refs. [29, 44, 45] we make a 20-dimensional fit, varying all the relevant $b \to s$ Wilson coefficients, thus, considering the most general description of NP effects in the $b \to s\ell\ell$ channel. We also established criteria to identify possible insensitive parameters and flat directions regarding NP. For another multidimensional approach considering the look-elsewhere effect see Ref. [46].

The results in Table 4 show that compared to our previous analyses [29, 34] we find now that the fit constrains all four parameters $C_{Q_1}^e, C_{Q_2}^e, C_{Q_1}^{e'}, C_{Q_2}^{e'}$ which previously were shown to be undetermined due to their large uncertainties in the previous analyses and negligible impact on the fit (resulting in the number of effective degrees of freedom to be 16). In Ref. [29] a criterion was presented to single out such undetermined parameters [3].

But also in the present fit the parameters C_{10}^e and $C_{10}^{e'}$ have larger uncertainties and can be shown to have a small impact on the fit. In addition one finds that there is degeneracy in the sense that the fit constrains the difference of these two WCs only, so for both WCs large values are possible. Removing one of the two WCs from the fit one finds the other one is well-constrained and does not effectively change the χ^2. Therefore we have 19 effective degrees of freedom.

The $\text{Pull}_{\rm SM}$ of the 20-parameter fit has increased by more than 2σ compared to the 2019 results. If we consider the fit with the 19 effective parameters we currently find a SM pull of 5.6σ.

The Wilks' test allows us to estimate the impact of the various parameters even further. The likelihood ratio test via Wilks' theorem enables us to estimate the significance of adding Wilson coefficients into a fit when one goes from one nested scenario to a more general one. In our previous analysis in Ref. [29] we found that adding Wilson coefficients to the "C_9^μ only" scenario was improving the fit only marginally.

[3] The precise criterion was given by the explicit check if the variation of each coefficient of order one, $|C_i| \sim 1$, implies/leads to $|\delta\chi^2| < 1$.

All observables with $\chi^2_{\rm SM} = 225.8$ $\chi^2_{\rm min} = 151.6$; $\quad \text{Pull}_{\rm SM} = 5.5(5.6)\sigma$			
δC_7 0.05 ± 0.03		δC_8 -0.70 ± 0.40	
$\delta C'_7$ -0.01 ± 0.02		$\delta C'_8$ 0.00 ± 0.80	
δC_9^{μ} -1.16 ± 0.17	δC_9^{e} -6.70 ± 1.20	δC_{10}^{μ} 0.20 ± 0.21	δC_{10}^{e} degenerate w/ C'^{e}_{10}
$\delta C'^{\mu}_9$ 0.09 ± 0.34	$\delta C'^{e}_9$ 1.90 ± 1.50	$\delta C'^{\mu}_{10}$ -0.12 ± 0.20	$\delta C'^{e}_{10}$ degenerate w/ C^{e}_{10}
$C^{\mu}_{Q_1}$ 0.04 ± 0.10 $[-0.08 \pm 0.11]$	$C^{e}_{Q_1}$ -1.50 ± 1.50 $[-0.20 \pm 1.60]$	$C^{\mu}_{Q_2}$ -0.09 ± 0.10 $[-0.11 \pm 0.10]$	$C^{e}_{Q_2}$ -4.10 ± 1.5 $[4.50 \pm 1.5]$
$C'^{\mu}_{Q_1}$ 0.15 ± 0.10 $[0.02 \pm 0.12]$	$C'^{e}_{Q_1}$ -1.70 ± 1.20 $[-0.30 \pm 1.10]$	$C'^{\mu}_{Q_2}$ -0.14 ± 0.11 $[-0.16 \pm 0.10]$	$C'^{e}_{Q_2}$ -4.20 ± 1.2 $[4.40 \pm 1.2]$

Table 4: Best fit values for the 20 operator global fit to the $b \to s$ data, assuming 10% error for the power corrections. The $\text{Pull}_{\rm SM}$ in the parenthesis corresponds considering 19 effective d.o.f. instead of 20. The numbers in the brackets refer to an alternative solution giving an equally good fit.

Set of WC	param.	$\chi^2_{\rm min}$	$\text{Pull}_{\rm SM}$	Improvement
SM	0	225.8	-	-
C_9^{μ}	1	168.6	7.6σ	7.6σ
C_9^{μ}, C_{10}^{μ}	2	167.5	7.3σ	1.0σ
$C_7, C_8, C_9^{(e,\mu)}, C_{10}^{(e,\mu)}$	6	158.0	7.1σ	2.0σ
All non-primed WC	10	157.2	6.5σ	0.1σ
All WC (incl. primed)	20 (19)	151.6	$5.5\,(5.6)\sigma$	$0.2\,(0.3)\sigma$

Table 5: $\text{Pull}_{\rm SM}$ of $1, 2, 6, 10$ and 20 dimensional fit. The "All non-primed WC" includes in addition to the previous row, the scalar and pseudoscalar Wilson coefficients. The last row also includes the chirality-flipped counterparts of the Wilson coefficients. In the last column the significance of improvement of the fit compared to the scenario of the previous row is given. The number in parentheses corresponds to the effective degrees of freedom (see the text for further details).

The Wilks' test with the present data shows that adding C_{10}^{μ} and C_9^{e}, C_{10}^{e} and also C_7 and C_8 improves the fit significantly and establishes the importance of these fit parameters (see Table 5). This can be explained by the fact that to a great degree, the tension and its increase compared to our previous analysis in Ref. [29] is due to the updated LFUV ratio R_K which can be described equally well by NP contributions to the electron and muon sectors. Furthermore, there is now more data on observables with electrons in the final state.

4 Future prospects and predictions for other ratios

Upgrades of the LHCb experiment are planned. The first upgrade will lead to a total integrated luminosity of 50 fb^{-1}. A second upgrade at a high-luminosity LHC will lead to an integrated luminosity of 300 fb^{-1}. We also use a third intermediate benchmark with an integrated luminosity of 18 fb^{-1} to analyse the future prospects of the clean observables R_K, R_{K^*} and $\text{BR}(B_s \to \mu^+\mu^-)$.

Our estimates of the future systematical uncertainties are based on the following considerations. From Table 2 in [21], the efficiency ratio between the electron mode and the muon mode is approximately one-third. The LHCb Upgrade will replace the hardware trigger by a software trigger which is expected to yield electron efficiencies closer to muon efficiencies (see Table 2 in [47]). We assume the efficiency ratio in the LHCb Upgrade grows from one-third to $\sim 60\%$. The ultimate systematic uncertainty for R_K is expected to be $\sim 1\%$ [48], and we assume that a similar ultimate systematic could hence be achieved for R_{K^*} (also in line with [49]). For the $B_s^0 \to \mu^+\mu^-$ branching fraction, two important systematic sources depend on external information : the value of the b-quark hadronisation fractions f_d/f_s, and the branching fraction of the $B^+ \to J/\psi(\to \mu^+\mu^-)K^+$ decay. Hence, an irreducible systematic of $\sim 4\%$ is assumed in our approach. We also assume that ATLAS, CMS, and LHCb will keep relative weights in the $B_s^0 \to \mu^+\mu^-$ branching fraction world average similar to the ones they currently have.

Considering the decrease in experimental uncertainties as described above we investigate the NP fits to the clean observables. Keeping the experimental central values as what they are currently do not give acceptable fits which is partly due to the different preferred NP scenarios for R_K and R_{K^*} in the [1.1,

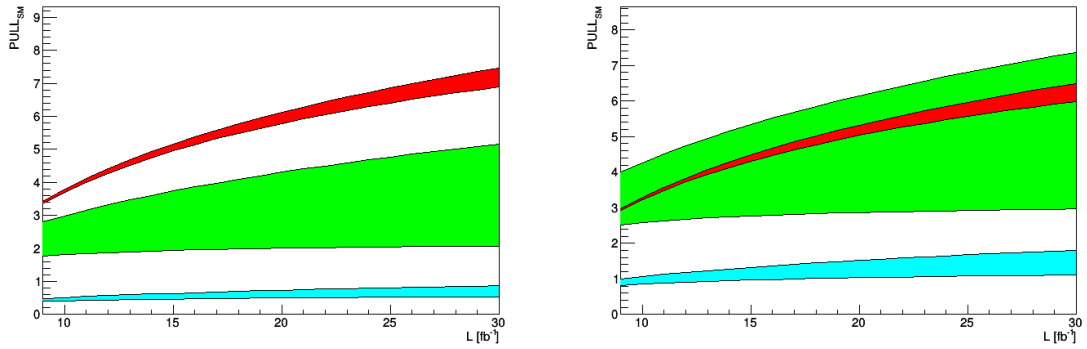

Figure 5: Significance of the tension between SM predictions and the experimental projections for LFUV observables, on the left [right] assuming current central value of C_9^μ [C_{10}^μ] from the clean observables (right panel of Table 1) remains unchanged. The red, green and blue band correspond to $R_K^{[1.1,6]}$, $R_{K^*}^{[1.1,6]}$ and $R_{K^*}^{[0.045,1.1]}$, respectively. The lower [upper] limit of each band corresponds to assuming the current systematic uncertainties do not improve [ultimate systematic uncertainty envisaged for the 50 fb^{-1} and 300 fb^{-1} luminosity] (see text for further details).

6] GeV^2 bin and partly due to the rather small value of R_{K^*} in the [0.045, 1.1] GeV^2 bin which cannot be reached with NP in the preferred NP scenarios. Instead we make a different but similarly strong assumption that future experimental results are in agreement with one of the current NP scenarios from the fit to clean observables.

Considering the three preferred scenarios of Table 1 we make projections for 18, 50 and 300 fb^{-1} luminosities. For the 18 fb^{-1} benchmark we assume 1.5, 3, 5 and 4.4% systematic uncertainties for $R_K([1.1,6])$, $R_{K^*}([0.045,1.1])$, $R_{K^*}([1.1,6])$ and BR($B_s \to \mu^+\mu^-$), respectively, while for the 50 and 300 fb^{-1} projections we consider the ultimate systematic uncertainty of 1% for all three LFUV ratios and 4% for BR($B_s \to \mu^+\mu^-$). In all three scenarios the NP significance will be larger than 6σ as given in Table 6.

Pull$_{\rm SM}$ with $R_{K^{(*)}}$ and BR($B_s \to \mu^+\mu^-$) prospects			
LHCb lum.	18 fb^{-1}	50 fb^{-1}	300 fb^{-1}
δC_9^μ	6.5σ	14.7σ	21.9σ
δC_{10}^μ	7.1σ	16.6σ	25.1σ
δC_{LL}^μ	7.5σ	17.7σ	26.6σ

Table 6: Predictions of Pull$_{\rm SM}$ for the fit to δC_9^μ, δC_{10}^μ and δC_{LL}^μ (as given in the right panel of Table 1) for the LHCb upgrade scenarios with 18, 50 and 300 fb^{-1} luminosity collected.

However, it should be noted that the significance is rather strongly dependent on the presumed systematic uncertainties as well as the considered scenario. This can be seen in Fig. 5 where Pull$_{\rm SM}$ for each LFUV ratios is individually shown for the C_9^μ and C_{10}^μ scenarios with different assumptions on the systematic uncertainties. For the C_9^μ case, R_K can individually reach 5σ significance at $\sim$ 16 fb^{-1} luminosity. On the one hand for the C_{10}^μ scenario, with the ultimate systematic uncertainty for $R_{K^*}([1.1,6])$ it gives 5σ Pull$_{\rm SM}$ at $\sim$ 13 fb^{-1}, however, assuming the current systematic uncertainty remains, it does not reach 3σ significance. On the other hand for the same C_{10}^μ scenario, with R_K, there is 5σ significance with $\sim$ 20 fb^{-1} luminosity and it is much less dependent on the assumption on the systematic error. In both scenarios $R_{K^*}([0.045,1.1])$ does not give a large Pull$_{\rm SM}$ as it is mostly dominated by C_7 and with the considered NP scenarios the predicted value for this bin (as given in the next paragraph) are very close to the SM prediction, 0.906 ± 0.028.

Nonetheless, a single LFUV observable cannot individually pinpoint the correct NP scenario. For example, the predicted 68% confidence interval with 9 fb^{-1} for the (very) low bin of R_{K^*} within the C_9^μ scenario is given by $([0.897, 0.874])$ $[0.853, 0.906]$ while for the C_{10}^μ scenario it is $([0.871, 0.889])$ $[0.793, 0.865]$ having overlapping intervals which prevents disentangling the preferred scenario. Considering the other four scenarios of Table 1 this problem becomes even more pronounced. The analytical dependence of the ratios on the NP-WCs given in Ref. [50] explain this feature. So it is expected that this feature stays valid also in future scenarios.

In Table 7 we give the 68% confidence interval predictions for other LFUV ratios of muons in the final state over electrons, assuming the various NP fits to $R_{K^{(*)}}$ and BR($B_s \to \mu^+\mu^-$) as given in the right panel of Table 1. There are a number of the ratios which are able to discern among the various scenarios (see also [51]). From the first row of Table 7, $R_{F_L}([1.1, 6])$ is predicted to have distinct intervals whether the considered scenario is NP in C_9^μ or C_{10}^μ, however there are still overlaps with other cases e.g. C_9^e which can be disentangled to some extent by considering further observables such as $R_{S_5}([1.1, 6])$.

	Predictions with best fit values of "clean" observables					
Obs.	C_9^μ	C_9^e	C_{10}^μ	C_{10}^e	C_{LL}^μ	C_{LL}^e
$R_{F_L}^{[1.1,6.0]}$	$[0.910, 0.943]$	$[0.935, 0.951]$	$[0.992, 1.001]$	$[0.993, 1.000]$	$[0.957, 0.968]$	$[1.000, 1.016]$
$R_{A_{FB}}^{[1.1,6.0]}$	$[3.909, 6.457]$	$[-0.572, -0.296]$	$[0.937, 0.939]$	$[0.953, 0.980]$	$[2.443, 3.488]$	$[0.244, 0.361]$
$R_{S_3}^{[1.1,6.0]}$	$[0.912, 0.942]$	$[0.900, 0.936]$	$[0.803, 0.880]$	$[0.841, 0.891]$	$[0.826, 0.895]$	$[1.020, 1.040]$
$R_{S_5}^{[1.1,6.0]}$	$[0.335, 0.650]$	$[0.697, 0.778]$	$[1.013, 1.014]$	$[1.030, 1.059]$	$[0.731, 0.840]$	$[1.213, 1.475]$
$R_{F_L}^{[15,19]}$	$[0.998, 0.999]$	$[0.998, 0.998]$	$[0.998, 0.998]$	$[0.998, 0.998]$	$[0.998, 0.998]$	$[0.998, 0.998]$
$R_{A_{FB}}^{[15,19]}$	$[0.908, 0.961]$	$[0.988, 0.992]$	$[1.007, 1.010]$	$[1.027, 1.053]$	$[0.995, 0.997]$	$[1.017, 1.036]$
$R_{S_3}^{[15,19]}$	$[0.998, 0.998]$	$[0.998, 0.998]$	$[0.999, 0.999]$	$[0.999, 0.999]$	$[0.999, 0.999]$	$[0.998, 0.998]$
$R_{S_5}^{[15,19]}$	$[0.908, 0.960]$	$[0.988, 0.992]$	$[1.007, 1.010]$	$[1.027, 1.053]$	$[0.995, 0.997]$	$[1.017, 1.036]$
$R_{K^*}^{[15,19]}$	$[0.798, 0.877]$	$[0.785, 0.868]$	$[0.803, 0.873]$	$[0.768, 0.853]$	$[0.773, 0.856]$	$[1.072, 1.128]$
$R_K^{[15,19]}$	$[0.795, 0.877]$	$[0.789, 0.871]$	$[0.833, 0.893]$	$[0.796, 0.874]$	$[0.791, 0.869]$	$[1.077, 1.135]$
$R_\phi^{[1.1,6.0]}$	$[0.843, 0.901]$	$[0.813, 0.887]$	$[0.799, 0.869]$	$[0.764, 0.850]$	$[0.792, 0.867]$	$[1.054, 1.096]$
$R_\phi^{[15,19]}$	$[0.799, 0.877]$	$[0.785, 0.868]$	$[0.801, 0.872]$	$[0.766, 0.853]$	$[0.772, 0.856]$	$[1.072, 1.128]$

Table 7: Predictions of LFUV observables at 68% confidence level, considering one operator fits obtained with the clean observables of Table 1. The observables $R_{K^{(*)}}$ and R_ϕ refer to the the branching fraction ratios of $B \to K^{(*)}\bar{\ell}\ell$ and $B_s \to \phi\bar{\ell}\ell$, respectively. The other observables correspond to ratios of the angular observables of the $B \to K^*\bar{\ell}\ell$ decay and the superscripts denote the q^2 bins.

In Table 8 and 9 we give the 1σ range predictions of these LFUV observables for the 18 and 50 fb^{-1} luminosity benchmarks, respectively where several of the observables give more distinct predictions for the various NP scenarios.

In Table 7, some of the observables such as $R_{A\mathrm{FB}}([1.1, 6])$ have a rather large uncertainty which is due to zero-crossings. In such cases, it is more suitable to consider observable differences ($O_i^\mu - O_i^e$) instead of ratios O_i^μ/O_i^e [52]. Similar observables are also defined for the optimised $P_i^{(\prime)}$ observables in [53]. In Appendix A, we give the prediction for the alternative set of observables in Tables 10, 11 and 12 for 9, 18 and 50 fb^{-1} luminosities, respectively.

	Predictions assuming 18 fb^{-1} luminosity					
Obs.	C_9^μ	C_9^e	C_{10}^μ	C_{10}^e	C_{LL}^μ	C_{LL}^e
$R_{F_L}^{[1.1,6.0]}$	$[0.916, 0.937]$	$[0.938, 0.947]$	$[0.993, 1.000]$	$[0.994, 0.999]$	$[0.959, 0.966]$	$[1.003, 1.013]$
$R_{A_{FB}}^{[1.1,6.0]}$	$[4.375, 5.954]$	$[-0.480, -0.323]$	$[0.938, 0.939]$	$[0.958, 0.975]$	$[2.611, 3.308]$	$[0.259, 0.333]$
$R_{S_3}^{[1.1,6.0]}$	$[0.917, 0.936]$	$[0.907, 0.929]$	$[0.813, 0.870]$	$[0.850, 0.880]$	$[0.838, 0.884]$	$[1.023, 1.036]$
$R_{S_5}^{[1.1,6.0]}$	$[0.398, 0.593]$	$[0.710, 0.759]$	$[1.013, 1.014]$	$[1.035, 1.053]$	$[0.750, 0.823]$	$[1.252, 1.417]$
$R_{F_L}^{[15,19]}$	$[0.998, 0.999]$	$[0.998, 0.998]$	$[0.998, 0.998]$	$[0.998, 0.998]$	$[0.998, 0.998]$	$[0.998, 0.998]$
$R_{A_{FB}}^{[15,19]}$	$[0.920, 0.952]$	$[0.988, 0.991]$	$[1.008, 1.010]$	$[1.032, 1.047]$	$[0.995, 0.996]$	$[1.020, 1.032]$
$R_{S_3}^{[15,19]}$	$[0.998, 0.998]$	$[0.998, 0.998]$	$[0.999, 0.999]$	$[0.999, 0.999]$	$[0.999, 0.999]$	$[0.998, 0.998]$
$R_{S_5}^{[15,19]}$	$[0.919, 0.952]$	$[0.988, 0.990]$	$[1.008, 1.010]$	$[1.032, 1.047]$	$[0.995, 0.996]$	$[1.020, 1.032]$
$R_{K^*}^{[15,19]}$	$[0.812, 0.861]$	$[0.800, 0.851]$	$[0.812, 0.863]$	$[0.784, 0.835]$	$[0.787, 0.842]$	$[1.082, 1.118]$
$R_K^{[15,19]}$	$[0.810, 0.861]$	$[0.804, 0.854]$	$[0.841, 0.885]$	$[0.811, 0.858]$	$[0.804, 0.856]$	$[1.087, 1.124]$
$R_\phi^{[1.1,6.0]}$	$[0.853, 0.889]$	$[0.827, 0.873]$	$[0.808, 0.859]$	$[0.780, 0.832]$	$[0.804, 0.854]$	$[1.062, 1.088]$
$R_\phi^{[15,19]}$	$[0.813, 0.861]$	$[0.800, 0.851]$	$[0.810, 0.862]$	$[0.783, 0.834]$	$[0.786, 0.842]$	$[1.082, 1.118]$

Table 8: Predictions of ratios at 68% confidence level for different scenarios, assuming the central values of Table 1 remains the same with 18 fb^{-1} luminosity. See the caption of Table 7 for more details.

	Predictions assuming 50 fb^{-1} luminosity					
Obs.	C_9^μ	C_9^e	C_{10}^μ	C_{10}^e	C_{LL}^μ	C_{LL}^e
$R_{F_L}^{[1.1,6.0]}$	$[0.922, 0.932]$	$[0.941, 0.944]$	$[0.995, 0.998]$	$[0.996, 0.997]$	$[0.961, 0.964]$	$[1.006, 1.010]$
$R_{A_{FB}}^{[1.1,6.0]}$	$[4.791, 5.520]$	$[-0.416, -0.358]$	$[0.938, 0.939]$	$[0.963, 0.970]$	$[2.822, 3.089]$	$[0.279, 0.307]$
$R_{S_3}^{[1.1,6.0]}$	$[0.922, 0.931]$	$[0.914, 0.922]$	$[0.832, 0.852]$	$[0.858, 0.870]$	$[0.853, 0.870]$	$[1.027, 1.032]$
$R_{S_5}^{[1.1,6.0]}$	$[0.453, 0.543]$	$[0.723, 0.742]$	$[1.014, 1.014]$	$[1.040, 1.048]$	$[0.773, 0.801]$	$[1.298, 1.361]$
$R_{F_L}^{[15,19]}$	$[0.998, 0.999]$	$[0.998, 0.998]$	$[0.998, 0.998]$	$[0.998, 0.998]$	$[0.998, 0.998]$	$[0.998, 0.998]$
$R_{A_{FB}}^{[15,19]}$	$[0.929, 0.944]$	$[0.988, 0.989]$	$[1.009, 1.010]$	$[1.036, 1.042]$	$[0.996, 0.996]$	$[1.023, 1.028]$
$R_{S_3}^{[15,19]}$	$[0.998, 0.998]$	$[0.998, 0.998]$	$[0.999, 0.999]$	$[0.999, 0.999]$	$[0.999, 0.999]$	$[0.998, 0.998]$
$R_{S_5}^{[15,19]}$	$[0.929, 0.944]$	$[0.988, 0.989]$	$[1.009, 1.010]$	$[1.036, 1.042]$	$[0.996, 0.996]$	$[1.023, 1.028]$
$R_{K^*}^{[15,19]}$	$[0.825, 0.847]$	$[0.815, 0.835]$	$[0.828, 0.846]$	$[0.799, 0.820]$	$[0.804, 0.825]$	$[1.093, 1.107]$
$R_K^{[15,19]}$	$[0.823, 0.847]$	$[0.819, 0.838]$	$[0.854, 0.870]$	$[0.825, 0.844]$	$[0.820, 0.839]$	$[1.098, 1.113]$
$R_\phi^{[1.1,6.0]}$	$[0.862, 0.879]$	$[0.841, 0.858]$	$[0.824, 0.843]$	$[0.795, 0.816]$	$[0.819, 0.839]$	$[1.070, 1.080]$
$R_\phi^{[15,19]}$	$[0.825, 0.847]$	$[0.815, 0.835]$	$[0.826, 0.845]$	$[0.797, 0.819]$	$[0.803, 0.824]$	$[1.093, 1.107]$

Table 9: Predictions of ratios at 68% confidence level for different scenarios, assuming the central values of Table 1 remains the same with 50 fb^{-1} luminosity. See the caption of Table 7 for more details.

5 Conclusions

The current experimental data on $b \to s$ transitions show deviations in several observables with respect to the Standard Model predictions. The latest LHCb update of the leptonic decay BR($B_s \to \mu^+\mu^-$) and the lepton flavour violating ratio R_K have further strengthened the New Physics description of the so-called B-anomalies which when taken together with the previously measured anomalies in the two bins of R_{K^*} results in more than 4σ significance.

Considering all available observables of $b \to s\ell\ell$ processes, the significance of the improved description of the data by New Physics contributions becomes even higher, this is however reliant on the assumptions made on the size of the not well-known power corrections in a number of observables of the exclusive $B \to K^{(*)}\ell\ell$ and $B_s \to \phi\ell\ell$ decays. In order to have an unbiased determination of the structure of New Physics contributions, we considered a 20-dimensional fit where all the relevant $b \to s$ operators are taken in account, still finding a large Pull$_{\rm SM}$. Interestingly, while in our previous analysis there was no significant indication of preference for going beyond one or two operator fits, we now see such an indication for considering simultaneously electron and muon contributions.

Assuming any of the favoured NP descriptions of the lepton-flavour universality violating observables remain, we show that New Physics can be established with more than 5σ significance already with 18 fb^{-1} of integrated luminosity. However, the preferred scenario, in general cannot be determined by only considering the $R_{K^{(*)}}$ observables. To disentangle the preferred New Physics scenario we also give predictions for further ratios with data already gathered by LHCb as well as the projected data with 18 and 50 fb^{-1} luminosity.

Acknowledgement

The work was supported by the Cluster of Excellence "Precision Physics, Fundamental Interactions, and Structure of Matter" (PRISMA$^+$ EXC 2118/1) funded by the German Research Foundation (DFG) within the German Excellence Strategy (Project ID 39083149), as well as BMBF Verbundprojekt 05H2018 - Belle II. TH thanks the CERN theory group for its hospitality during his regular visits to CERN where part of the work was done. This work has received financial support from Xunta de Galicia (Centro singular de investigación de Galicia accreditation 2019-2022), by European Union ERDF, and by the "María de Maeztu" Units of Excellence program MDM-2016-0692 and the Spanish Research State Agency.

A Predictions for further LFUV observables

	Predictions with best fit values of "clean" observables					
Obs.	C_9^μ	C_9^e	C_{10}^μ	C_{10}^e	C_{LL}^μ	C_{LL}^e
$D_{F_L}^{[1.1,6.0]}$	$[-0.069, -0.043]$	$[-0.052, -0.039]$	$[-0.006, 0.001]$	$[-0.005, 0.000]$	$[-0.032, -0.025]$	$[0.000, 0.012]$
$D_{A_{FB}}^{[1.1,6.0]}$	$[-0.074, -0.039]$	$[-0.055, -0.034]$	$[0.001, 0.001]$	$[0.000, 0.001]$	$[-0.034, -0.019]$	$[0.022, 0.039]$
$D_{S_3}^{[1.1,6.0]}$	$[0.001, 0.001]$	$[0.001, 0.001]$	$[0.001, 0.002]$	$[0.001, 0.002]$	$[0.001, 0.002]$	$[0.000, 0.000]$
$D_{S_4}^{[1.1,6.0]}$	$[-0.003, -0.003]$	$[-0.009, -0.005]$	$[-0.028, -0.017]$	$[-0.027, -0.018]$	$[-0.020, -0.012]$	$[0.000, 0.000]$
$D_{S_5}^{[1.1,6.0]}$	$[0.057, 0.108]$	$[0.046, 0.071]$	$[-0.002, -0.002]$	$[-0.009, -0.005]$	$[0.026, 0.044]$	$[-0.052, -0.028]$
$D_{F_L}^{[15,19]}$	$[-0.001, 0.000]$	$[-0.001, -0.001]$	$[-0.001, -0.001]$	$[-0.001, -0.001]$	$[-0.001, -0.001]$	$[-0.001, -0.001]$
$D_{A_{FB}}^{[15,19]}$	$[-0.035, -0.015]$	$[-0.005, -0.003]$	$[0.003, 0.004]$	$[0.010, 0.019]$	$[-0.002, -0.001]$	$[0.006, 0.013]$
$D_{S_3}^{[15,19]}$	$[0.000, 0.000]$	$[0.000, 0.000]$	$[0.000, 0.000]$	$[0.000, 0.000]$	$[0.000, 0.000]$	$[0.000, 0.000]$
$D_{S_4}^{[15,19]}$	$[0.000, 0.000]$	$[-0.001, -0.001]$	$[-0.001, -0.001]$	$[-0.001, 0.000]$	$[-0.001, -0.001]$	$[-0.001, -0.001]$
$D_{S_5}^{[15,19]}$	$[0.011, 0.026]$	$[0.002, 0.004]$	$[-0.003, -0.002]$	$[-0.014, -0.007]$	$[0.001, 0.001]$	$[-0.010, -0.005]$
$R_{P_2}^{[1.1,6.0]}$	$[3.557, 5.358]$	$[-0.526, -0.255]$	$[0.998, 1.030]$	$[1.012, 1.063]$	$[2.397, 3.320]$	$[0.277, 0.392]$
$R_{P_1}^{[1.1,6.0]}$	$[0.757, 0.858]$	$[0.778, 0.000]$	$[0.881, 0.936]$	$[0.912, 0.945]$	$[0.786, 0.878]$	$[1.105, 1.180]$
$R_{P_4}^{[1.1,6.0]}$	$[0.934, 0.959]$	$[0.902, -0.039]$	$[0.821, 0.899]$	$[0.862, 0.910]$	$[0.845, 0.912]$	$[1.039, 1.059]$
$R_{P_5}^{[1.1,6.0]}$	$[0.320, 0.638]$	$[0.670, -0.034]$	$[1.049, 1.062]$	$[1.065, 1.103]$	$[0.729, 0.846]$	$[1.263, 1.559]$
$R_{P_2}^{[15,19]}$	$[0.909, 0.962]$	$[0.990, 0.001]$	$[1.010, 1.012]$	$[1.029, 1.055]$	$[0.997, 0.999]$	$[1.019, 1.038]$
$R_{P_1}^{[15,19]}$	$[1.000, 1.000]$	$[1.000, -0.005]$	$[1.001, 1.001]$	$[1.001, 1.001]$	$[1.000, 1.001]$	$[1.000, 1.000]$
$R_{P_4}^{[15,19]}$	$[1.000, 1.000]$	$[1.000, 0.071]$	$[1.000, 1.000]$	$[1.000, 1.000]$	$[1.000, 1.000]$	$[1.000, 1.000]$
$R_{P_5}^{[15,19]}$	$[0.909, 0.962]$	$[0.989, -0.001]$	$[1.010, 1.012]$	$[1.029, 1.055]$	$[0.997, 0.999]$	$[1.019, 1.038]$
$Q_2^{[1.1,6.0]}$	$[0.096, 0.164]$	$[0.103, 0.174]$	$[0.000, 0.001]$	$[0.000, 0.002]$	$[0.053, 0.087]$	$[-0.093, -0.055]$
$Q_1^{[1.1,6.0]}$	$[0.014, 0.024]$	$[0.016, 0.029]$	$[0.006, 0.012]$	$[0.006, 0.010]$	$[0.012, 0.021]$	$[-0.015, -0.010]$
$Q_4^{[1.1,6.0]}$	$[-0.041, -0.025]$	$[-0.068, -0.036]$	$[-0.110, -0.062]$	$[-0.100, -0.061]$	$[-0.095, -0.054]$	$[0.023, 0.035]$
$Q_5^{[1.1,6.0]}$	$[0.138, 0.259]$	$[0.119, 0.191]$	$[-0.024, -0.019]$	$[-0.036, -0.024]$	$[0.059, 0.104]$	$[-0.139, -0.081]$
$Q_2^{[15,19]}$	$[0.014, 0.034]$	$[0.002, 0.004]$	$[-0.004, -0.004]$	$[-0.020, -0.011]$	$[0.001, 0.001]$	$[-0.014, -0.007]$
$Q_1^{[15,19]}$	$[0.000, 0.000]$	$[0.000, 0.000]$	$[-0.001, 0.000]$	$[-0.001, 0.000]$	$[0.000, 0.000]$	$[0.000, 0.000]$
$Q_4^{[15,19]}$	$[0.000, 0.000]$	$[0.000, 0.000]$	$[0.000, 0.000]$	$[0.000, 0.000]$	$[0.000, 0.000]$	$[0.000, 0.000]$
$Q_5^{[15,19]}$	$[0.023, 0.055]$	$[0.004, 0.006]$	$[-0.007, -0.006]$	$[-0.031, -0.017]$	$[0.001, 0.002]$	$[-0.022, -0.011]$

Table 10: Predictions of ratios and differences of observables with muons in the final state to electrons in the final state at 68% confidence level, considering one operator fits obtained with the clean observables of Table 1. The observables $D_{S_{3,4,5}} = S_{3,4,5}^\mu - S_{3,4,5}^e$, $D_{A_{FB}} = A_{FB}^\mu - A_{FB}^e$, $D_{F_L} = Q_{F_L} = F_L^\mu - F_L^e$ and $Q_{1,2,4,5} = P_{1,2,4,5}^{(\prime)\,\mu} - P_{1,2,4,5}^{(\prime)\,e}$ and $R_{P_i} = P_{1,2,4,5}^{(\prime)\,\mu}/P_{1,2,4,5}^{(\prime)\,e}$ all correspond to the $B \to K^* \bar{\ell}\ell$ decay. The observables $R_{K^{(*)}}$, R_{X_s} and R_ϕ correspond to the ratios of the branching fractions of $B \to K^{(*)}\bar{\ell}\ell$, $B \to X_s\bar{\ell}\ell$ and $B_s \to \phi\bar{\ell}\ell$, respectively. The superscripts denote the q^2 bins.

	Predictions assuming 18 fb^{-1} luminosity					
Obs.	C_9^μ	C_9^e	C_{10}^μ	C_{10}^e	C_{LL}^μ	C_{LL}^e
$D_{F_L}^{[1.1,6.0]}$	$[-0.064, -0.048]$	$[-0.049, -0.041]$	$[-0.005, 0.000]$	$[-0.004, -0.001]$	$[-0.031, -0.026]$	$[0.002, 0.010]$
$D_{A_{FB}}^{[1.1,6.0]}$	$[-0.067, -0.046]$	$[-0.051, -0.038]$	$[0.001, 0.001]$	$[0.000, 0.001]$	$[-0.031, -0.022]$	$[0.025, 0.036]$
$D_{S_3}^{[1.1,6.0]}$	$[0.001, 0.001]$	$[0.001, 0.001]$	$[0.002, 0.002]$	$[0.002, 0.002]$	$[0.001, 0.002]$	$[0.000, 0.000]$
$D_{S_4}^{[1.1,6.0]}$	$[-0.003, -0.003]$	$[-0.008, -0.006]$	$[-0.027, -0.019]$	$[-0.025, -0.020]$	$[-0.019, -0.014]$	$[0.000, 0.000]$
$D_{S_5}^{[1.1,6.0]}$	$[0.066, 0.098]$	$[0.051, 0.066]$	$[-0.002, -0.002]$	$[-0.008, -0.006]$	$[0.029, 0.041]$	$[-0.048, -0.033]$
$D_{F_L}^{[15,19]}$	$[-0.001, 0.000]$	$[-0.001, -0.001]$	$[-0.001, -0.001]$	$[-0.001, -0.001]$	$[-0.001, -0.001]$	$[-0.001, -0.001]$
$D_{A_{FB}}^{[15,19]}$	$[-0.030, -0.018]$	$[-0.005, -0.004]$	$[0.003, 0.004]$	$[0.012, 0.017]$	$[-0.002, -0.001]$	$[0.007, 0.012]$
$D_{S_3}^{[15,19]}$	$[0.000, 0.000]$	$[0.000, 0.000]$	$[0.000, 0.000]$	$[0.000, 0.000]$	$[0.000, 0.000]$	$[0.000, 0.000]$
$D_{S_4}^{[15,19]}$	$[0.000, 0.000]$	$[-0.001, -0.001]$	$[-0.001, -0.001]$	$[-0.001, 0.000]$	$[-0.001, -0.001]$	$[-0.001, -0.001]$
$D_{S_5}^{[15,19]}$	$[0.014, 0.023]$	$[0.003, 0.004]$	$[-0.003, -0.002]$	$[-0.013, -0.009]$	$[0.001, 0.001]$	$[-0.009, -0.006]$
$R_{P_2}^{[1.1,6.0]}$	$[3.914, 5.029]$	$[-0.436, -0.282]$	$[1.002, 1.026]$	$[1.022, 1.053]$	$[2.551, 3.166]$	$[0.292, 0.364]$
$R_{P_1}^{[1.1,6.0]}$	$[0.775, 0.837]$	$[0.792, 0.000]$	$[0.889, 0.930]$	$[0.918, 0.938]$	$[0.802, 0.863]$	$[1.118, 1.166]$
$R_{P_4}^{[1.1,6.0]}$	$[0.937, 0.953]$	$[0.910, -0.041]$	$[0.832, 0.889]$	$[0.871, 0.900]$	$[0.857, 0.902]$	$[1.043, 1.056]$
$R_{P_5}^{[1.1,6.0]}$	$[0.383, 0.580]$	$[0.685, -0.038]$	$[1.051, 1.060]$	$[1.072, 1.095]$	$[0.749, 0.827]$	$[1.307, 1.494]$
$R_{P_2}^{[15,19]}$	$[0.921, 0.954]$	$[0.990, 0.001]$	$[1.010, 1.012]$	$[1.034, 1.049]$	$[0.997, 0.998]$	$[1.022, 1.034]$
$R_{P_1}^{[15,19]}$	$[1.000, 1.000]$	$[1.000, -0.006]$	$[1.001, 1.001]$	$[1.001, 1.001]$	$[1.000, 1.001]$	$[1.000, 1.000]$
$R_{P_4}^{[15,19]}$	$[1.000, 1.000]$	$[1.000, 0.066]$	$[1.000, 1.000]$	$[1.000, 1.000]$	$[1.000, 1.000]$	$[1.000, 1.000]$
$R_{P_5}^{[15,19]}$	$[0.921, 0.954]$	$[0.990, -0.001]$	$[1.010, 1.012]$	$[1.033, 1.049]$	$[0.997, 0.998]$	$[1.022, 1.034]$
$Q_2^{[1.1,6.0]}$	$[0.110, 0.152]$	$[0.117, 0.161]$	$[0.000, 0.001]$	$[0.001, 0.002]$	$[0.058, 0.082]$	$[-0.086, -0.062]$
$Q_1^{[1.1,6.0]}$	$[0.016, 0.023]$	$[0.019, 0.027]$	$[0.007, 0.011]$	$[0.007, 0.009]$	$[0.014, 0.020]$	$[-0.014, -0.011]$
$Q_4^{[1.1,6.0]}$	$[-0.039, -0.029]$	$[-0.062, -0.042]$	$[-0.104, -0.069]$	$[-0.092, -0.069]$	$[-0.088, -0.061]$	$[0.026, 0.033]$
$Q_5^{[1.1,6.0]}$	$[0.160, 0.235]$	$[0.134, 0.178]$	$[-0.023, -0.019]$	$[-0.034, -0.026]$	$[0.066, 0.096]$	$[-0.128, -0.091]$
$Q_2^{[15,19]}$	$[0.017, 0.030]$	$[0.003, 0.004]$	$[-0.004, -0.004]$	$[-0.018, -0.012]$	$[0.001, 0.001]$	$[-0.012, -0.008]$
$Q_1^{[15,19]}$	$[0.000, 0.000]$	$[0.000, 0.000]$	$[-0.001, -0.001]$	$[-0.001, -0.001]$	$[0.000, 0.000]$	$[0.000, 0.000]$
$Q_4^{[15,19]}$	$[0.000, 0.000]$	$[0.000, 0.000]$	$[0.000, 0.000]$	$[0.000, 0.000]$	$[0.000, 0.000]$	$[0.000, 0.000]$
$Q_5^{[15,19]}$	$[0.028, 0.048]$	$[0.005, 0.006]$	$[-0.007, -0.006]$	$[-0.028, -0.020]$	$[0.001, 0.002]$	$[-0.020, -0.013]$

Table 11: Predictions of ratios of observables with muons in the final state to electrons in the final state at 68% confidence level for different scenarios, assuming the the central values of Table 1 remains the same with 18 fb^{-1} luminosity. For the definition of the observables see the caption of Table 10.

	Predictions assuming 50 fb^{-1} luminosity					
Obs.	C_9^μ	C_9^e	C_{10}^μ	C_{10}^e	C_{LL}^μ	C_{LL}^e
$D_{F_L}^{[1.1,6.0]}$	$[-0.059, -0.052]$	$[-0.047, -0.044]$	$[-0.004, -0.002]$	$[-0.003, -0.002]$	$[-0.029, -0.027]$	$[0.004, 0.007]$
$D_{A_{FB}}^{[1.1,6.0]}$	$[-0.061, -0.051]$	$[-0.047, -0.042]$	$[0.001, 0.001]$	$[0.000, 0.000]$	$[-0.028, -0.025]$	$[0.028, 0.032]$
$D_{S_3}^{[1.1,6.0]}$	$[0.001, 0.001]$	$[0.001, 0.001]$	$[0.002, 0.002]$	$[0.002, 0.002]$	$[0.002, 0.002]$	$[0.000, 0.000]$
$D_{S_4}^{[1.1,6.0]}$	$[-0.003, -0.003]$	$[-0.007, -0.006]$	$[-0.024, -0.021]$	$[-0.024, -0.021]$	$[-0.017, -0.015]$	$[0.000, 0.000]$
$D_{S_5}^{[1.1,6.0]}$	$[0.074, 0.089]$	$[0.056, 0.062]$	$[-0.002, -0.002]$	$[-0.007, -0.006]$	$[0.032, 0.037]$	$[-0.043, -0.037]$
$D_{F_L}^{[15,19]}$	$[-0.001, 0.000]$	$[-0.001, -0.001]$	$[-0.001, -0.001]$	$[-0.001, -0.001]$	$[-0.001, -0.001]$	$[-0.001, -0.001]$
$D_{A_{FB}}^{[15,19]}$	$[-0.027, -0.021]$	$[-0.004, -0.004]$	$[0.003, 0.004]$	$[0.013, 0.015]$	$[-0.002, -0.001]$	$[0.009, 0.010]$
$D_{S_3}^{[15,19]}$	$[0.000, 0.000]$	$[0.000, 0.000]$	$[0.000, 0.000]$	$[0.000, 0.000]$	$[0.000, 0.000]$	$[0.000, 0.000]$
$D_{S_4}^{[15,19]}$	$[0.000, 0.000]$	$[-0.001, -0.001]$	$[-0.001, -0.001]$	$[-0.001, -0.001]$	$[-0.001, -0.001]$	$[-0.001, -0.001]$
$D_{S_5}^{[15,19]}$	$[0.016, 0.020]$	$[0.003, 0.003]$	$[-0.003, -0.003]$	$[-0.012, -0.010]$	$[0.001, 0.001]$	$[-0.008, -0.006]$
$R_{P_2}^{[1.1,6.0]}$	$[4.221, 4.736]$	$[-0.373, -0.316]$	$[1.010, 1.018]$	$[1.031, 1.044]$	$[2.740, 2.976]$	$[0.311, 0.338]$
$R_{P_1}^{[1.1,6.0]}$	$[0.791, 0.820]$	$[0.807, 0.000]$	$[0.902, 0.917]$	$[0.924, 0.932]$	$[0.821, 0.845]$	$[1.133, 1.151]$
$R_{P_4}^{[1.1,6.0]}$	$[0.941, 0.948]$	$[0.918, -0.044]$	$[0.850, 0.871]$	$[0.879, 0.891]$	$[0.871, 0.888]$	$[1.047, 1.052]$
$R_{P_5}^{[1.1,6.0]}$	$[0.437, 0.528]$	$[0.701, -0.042]$	$[1.054, 1.058]$	$[1.079, 1.088]$	$[0.774, 0.804]$	$[1.359, 1.430]$
$R_{P_2}^{[15,19]}$	$[0.931, 0.946]$	$[0.990, 0.001]$	$[1.011, 1.012]$	$[1.038, 1.044]$	$[0.997, 0.998]$	$[1.025, 1.030]$
$R_{P_1}^{[15,19]}$	$[1.000, 1.000]$	$[1.000, -0.006]$	$[1.001, 1.001]$	$[1.001, 1.001]$	$[1.000, 1.001]$	$[1.000, 1.000]$
$R_{P_4}^{[15,19]}$	$[1.000, 1.000]$	$[1.000, 0.062]$	$[1.000, 1.000]$	$[1.000, 1.000]$	$[1.000, 1.000]$	$[1.000, 1.000]$
$R_{P_5}^{[15,19]}$	$[0.930, 0.946]$	$[0.990, -0.001]$	$[1.011, 1.012]$	$[1.038, 1.044]$	$[0.997, 0.998]$	$[1.025, 1.030]$
$Q_2^{[1.1,6.0]}$	$[0.121, 0.141]$	$[0.131, 0.148]$	$[0.000, 0.001]$	$[0.001, 0.001]$	$[0.066, 0.074]$	$[-0.079, -0.069]$
$Q_1^{[1.1,6.0]}$	$[0.018, 0.021]$	$[0.021, 0.024]$	$[0.008, 0.010]$	$[0.007, 0.008]$	$[0.016, 0.018]$	$[-0.013, -0.012]$
$Q_4^{[1.1,6.0]}$	$[-0.036, -0.032]$	$[-0.056, -0.048]$	$[-0.092, -0.079]$	$[-0.086, -0.076]$	$[-0.080, -0.069]$	$[0.028, 0.031]$
$Q_5^{[1.1,6.0]}$	$[0.180, 0.215]$	$[0.148, 0.165]$	$[-0.022, -0.021]$	$[-0.031, -0.028]$	$[0.075, 0.086]$	$[-0.117, -0.102]$
$Q_2^{[15,19]}$	$[0.021, 0.026]$	$[0.003, 0.004]$	$[-0.004, -0.004]$	$[-0.016, -0.014]$	$[0.001, 0.001]$	$[-0.011, -0.009]$
$Q_1^{[15,19]}$	$[0.000, 0.000]$	$[0.000, 0.000]$	$[-0.001, -0.001]$	$[-0.001, -0.001]$	$[0.000, 0.000]$	$[0.000, 0.000]$
$Q_4^{[15,19]}$	$[0.000, 0.000]$	$[0.000, 0.000]$	$[0.000, 0.000]$	$[0.000, 0.000]$	$[0.000, 0.000]$	$[0.000, 0.000]$
$Q_5^{[15,19]}$	$[0.033, 0.042]$	$[0.005, 0.006]$	$[-0.007, -0.007]$	$[-0.026, -0.022]$	$[0.001, 0.002]$	$[-0.018, -0.015]$

Table 12: Predictions of ratios of observables with muons in the final state to electrons in the final state at 68% confidence level for different scenarios, assuming the the central values of Table 1 remains the same with 50 fb^{-1} luminosity. For the definition of the observables see the caption of Table 10.

References

[1] LHCb collaboration, R. Aaij et al., *Phys. Rev. Lett.* **111** (2013) 191801, [1308.1707].

[2] S. Descotes-Genon, J. Matias and J. Virto, *Phys. Rev.* **D88** (2013) 074002, [1307.5683].

[3] W. Altmannshofer and D. M. Straub, *Eur. Phys. J.* **C73** (2013) 2646, [1308.1501].

[4] F. Beaujean, C. Bobeth and D. van Dyk, *Eur. Phys. J.* **C74** (2014) 2897, [1310.2478].

[5] R. R. Horgan, Z. Liu, S. Meinel and M. Wingate, *Phys. Rev. Lett.* **112** (2014) 212003, [1310.3887].

[6] T. Hurth and F. Mahmoudi, *JHEP* **04** (2014) 097, [1312.5267].

[7] LHCb collaboration, R. Aaij et al., *JHEP* **02** (2016) 104, [1512.04442].

[8] LHCb collaboration, R. Aaij et al., *Phys. Rev. Lett.* **125** (2020) 011802, [2003.04831].

[9] LHCb collaboration, R. Aaij et al., *JHEP* **09** (2015) 179, [1506.08777].

[10] G. Hiller and F. Kruger, *Phys. Rev.* **D69** (2004) 074020, [hep-ph/0310219].

[11] M. Bordone, G. Isidori and A. Pattori, *Eur. Phys. J.* **C76** (2016) 440, [1605.07633].

[12] LHCb collaboration, R. Aaij et al., *Phys. Rev. Lett.* **113** (2014) 151601, [1406.6482].

[13] LHCb collaboration, R. Aaij et al., *Phys. Rev. Lett.* **122** (2019) 191801, [1903.09252].

[14] LHCb collaboration, R. Aaij et al., *JHEP* **08** (2017) 055, [1705.05802].

[15] R. Alonso, B. Grinstein and J. Martin Camalich, Phys. Rev. Lett. **113** (2014), 241802, [1407.7044].

[16] G. Hiller and M. Schmaltz, Phys. Rev. D **90** (2014), 054014, [1408.1627].

[17] T. Hurth, F. Mahmoudi and S. Neshatpour, JHEP **12** (2014), 053, [1410.4545].

[18] W. Altmannshofer and D. M. Straub, Eur. Phys. J. C **75** (2015) no.8, 382, [1411.3161].

[19] LHCb collaboration, R. Aaij et al., [2108.09283].

[20] LHCb collaboration, R. Aaij et al., [2108.09284].

[21] LHCb collaboration, R. Aaij et al., 2103.11769.

[22] ATLAS collaboration, M. Aaboud et al., *JHEP* **04** (2019) 098, [1812.03017].

[23] CMS collaboration, A. M. Sirunyan et al., *JHEP* **04** (2020) 188, [1910.12127].

[24] S. Jäger and J. Martin Camalich, *JHEP* **05** (2013)043, [1212.2263]

[25] S. Jäger and J. Martin Camalich, *Phys. Rev.* **D93** (2016) 014028, [1412.3183].

[26] M. Ciuchini, M. Fedele, E. Franco, S. Mishima, A. Paul, L. Silvestrini and M. Valli, *JHEP* **06** (2016)116, [1512.07157]

[27] V. G. Chobanova, T. Hurth, F. Mahmoudi, D. Martinez Santos and S. Neshatpour, *JHEP* **07** (2017)025, [1702.02234]

[28] M. Ciuchini, A. M. Coutinho, M. Fedele, E. Franco, A. Paul, L. Silvestrini and M. Valli, *Eur. Phys. J.* **C77** (2017) 688, [1704.05447].

[29] A. Arbey, T. Hurth, F. Mahmoudi and S. Neshatpour, *Phys. Rev.* **D98** (2018) 095027, [1806.02791].

[30] C. Bobeth, M. Chrzaszcz, D. van Dyk and J. Virto, *Eur. Phys. J.* **C78** (2018) 451, [1707.07305].

[31] N. Gubernari, D. Van Dyk and J. Virto, *JHEP* **04** (2020) 188, [2011.09813].

[32] A. Abdesselam *et al.* [Belle], *Phys. Rev. Lett.* **126** (2021) 161801, [1904.02440].

[33] F. Mahmoudi, Comput. Phys. Commun. **178** (2008) 745 [0710.2067]; Comput. Phys. Commun. **180** (2009) 1579 [0808.3144]; Comput. Phys. Commun. **180** (2009) 1718.

[34] A. Arbey, T. Hurth, F. Mahmoudi, D. M. Santos and S. Neshatpour, *Phys. Rev.* **D100** (2019) 015045, [1904.08399].

[35] L. S. Geng, B. Grinstein, S. Jäger, S. Y. Li, J. Martin Camalich and R. X. Shi, [2103.12738].

[36] W. Altmannshofer and P. Stangl, [2103.13370].

[37] M. Algueró, B. Capdevila, S. Descotes-Genon, J. Matias and M. Novoa-Brunet, [2104.08921].

[38] A. Angelescu, D. Bečirević, D. A. Faroughy, F. Jaffredo and O. Sumensari, [2103.12504].

[39] T. Hurth, F. Mahmoudi and S. Neshatpour, *Phys. Rev.* **D102** (2020) 055001, [2006.04213].

[40] T. Hurth, F. Mahmoudi and S. Neshatpour, [2012.12207].

[41] A. K. Alok, A. Dighe, S. Gangal and D. Kumar, *JHEP* **06** (2019)089, [1903.09617]

[42] G. Cacciapaglia, C. Cot and F. Sannino, [2104.08818]

[43] T. Hurth, F. Mahmoudi and S. Neshatpour, Nucl. Phys. B **909** (2016), 737-777, [1603.00865].

[44] F. Mahmoudi, T. Hurth and S. Neshatpour, *Acta. Phys. Polon. B* **49** (2018) 1267.

[45] T. Hurth, A. Arbey, F. Mahmoudi and S. Neshatpour, Nucl. Part. Phys. Proc. **303-305** (2018), 2-7, [1812.07602].

[46] D. Lancierini, G. Isidori, P. Owen and N. Serra, [2104.05631].

[47] R. Aaij *et al.* Comput. Softw. Big Sci. **4** (2020) no.1, 7, [1912.09161].

[48] Talk given by K. Petridis for the LHCb collaboration on 23 March 2021, https://indi.to/MrPBJ.

[49] LHCb Collaboration, R. Aaij et al. , Tech. Rep. CERN-LHCC-2017-003, CERN, Geneva, Feb, 2017.

[50] G. D'Amico, M. Nardecchia, P. Panci, F. Sannino, A. Strumia, R. Torre et al., *JHEP* **09** (2017) 010, [1704.05438].

[51] T. Hurth, F. Mahmoudi, D. Martinez Santos and S. Neshatpour, *Phys. Rev.* **D96** (2017) 095034, [1705.06274].

[52] W. Altmannshofer and I. Yavin, *Phys. Rev.* **D92** (2015) 075022, [1508.07009].

[53] B. Capdevila, S. Descotes-Genon, J. Matias and J. Virto, *JHEP* **10** (2016) 075, [1605.03156].